Electronic Supplementary Material (ESI) for Journal of Materials Chemistry A.

Supporting Information

Solar and Thermal Multi-Sensing Microfiber Supercapacitor with Intelligent Self-Conditioned Capacitance and Body Temperature Monitoring

Youchao Teng [a], Jing Wei [a], Hongbiao Du [b], Mansoorianfar Mojtaba [a], Dagang Li [a, *]

a. College of Materials Science and Engineering, Nanjing Forestry University, 159 Longpan Road, Nanjing, Jiangsu, China

b. College of Environment and Natural Resources, Renmin University of China, No. 59, Zhongguancun Street, 100872 Beijing, People's Republic of China

* Corresponding author: njfuldg@163.com. (D. Li)

Table of contents

Experimental

Synthesis

Preparation of Graphene Oxide Aqueous Phase Dispersion. Graphene oxide (GO) was obtained by oxidizing commercial graphite according to improved Hummer's method.[1,2] Specifically, 1.0 g of scaly natural graphite was added to a 150 mL three-neck round bottom flask, slowly 30 mL of concentrated sulfuric acid was added while stirring at room temperature. After stirring in a low-temperature water bath (0 °C) with a Teflon paddle at 300 rpm for 1.0 h. 3.0 g of potassium permanganate powder was slowly added. The temperature of the reaction system was kept carefully would not exceed 20 °C in the flask. Furthermore, 10 mL of Milli-Q water was slowly added dropwise to the flask, and the temperature of the system was slowly raised to 95 °C; the reaction continued until it was completed. The reaction solution was slowly added to a beaker containing 500 mL of an ice-water mixture, then 10 mL of hydrogen peroxide (30%) was added dropwise, and the system turned from brown to yellow. The product was taken up and washed 5 times with 10% hydrochloric acid, then rinsed with Milli-Q water to remove hydrochloric acid. Finally, it was diluted with Milli-Q water and repeatedly centrifuged to remove unreacted particulate matter until the pH of the supernatant reached neutral 10 mL of graphene oxide solution was taken, and the sample with a frozen dryer and the solution concentration was measured. The graphene oxide solution was stored in the dark for use.

Preparation of Cellulose Nanofibrils. Cellulose nanofibrils (CNFs) were extracted from the pine powders by chemical and mechanical methods according to previous reports.[3,4] First, 20 g of pine powders were placed in a vacuum oven and dried overnight.

Then, the pine powders were treated with 1.0 wt.% sodium hypochlorite solution at 70 °C for 2 h and then washed with Milli-Q water until the pH of the supernatant reached neutral. This process was repeated 5 times to remove lignin. Next, the hemicellulose present in the sample was removed using 6 wt.% hydroxide solution at 85 °C for 2 h. Finally, a water slurry with 1.0 wt.% purified sample was passed 6 times through a grinder (MKCA6-2; Masuku Sangyo Co., Ltd., Japan) at 1200 rpm. By adjusting the distance between the upper and lower grindstones of the grinder to 0.3 mm, the purified cellulose fibrils were fibrillated into CNFs through high-speed shearing and extrusion during the rotation of the grindstones.

Preparation of Core-Sheath GE@PANI Microfibers. GE@PANI microfibers were fabricated by chemical in-situ polymerization. The experimental methods and process have been consistent with the GE/CNFs@PANI microfibers.

Analysis

Research on Comprehensive Properties of GE/CNFs Core Microfibers with Different CNFs Contents

As is known to all, microfiber electrodes have excellent hydrophilicity beneficial for promoting electrolyte penetration.[5] Therefore, it is essential to improve the hydrophilicity of the graphene-based microfiber electrodes to achieve improved electrochemical performance. **Figure S1c** shows the contact angle of the GE/CNFs hybrid microfibers. The GE microfiber exhibited typical hydrophobicity with a contact angle of 106°. Conversely, as the hydrophilic units CNFs ratios of GE from 1:0 increase to 1:1, contact angles drop to 90°, 75°, 51.5° and 43.9°, which is shown that the CNFs could effectively improve the hydrophilic of GE microfibers.

The conductivity of the GE and GE/CNFs microfibers and schematic diagram of the conductivity test are given in **Figure S1a, b**. The conductivity only changed subtlety from 80.5 S cm^{-1} to 47.2 S cm^{-1}, indicating excellent conductivity retention of GE/CNFs microfibers. XRD pattern **(Figure S2a)** of the GE microfiber shows clear diffraction peaks related to graphene basal planes. The peak at 24.32° (d-spacing of 3.74 Å) corresponds to (0 0 2) planes of GE. This peak moved from 24.32° to 23.64° as CNFs loading increased from 0 to 50%, corresponding to a shift in the (0 0 2) planes' distance from 3.74 to 3.84 Å. These results suggest a substantial number of CNFs incorporated into nanocomposites as a function of CNFs content, which is in agreement with the data of conductivity and contact angles **(Figure S1 b, c)**.

Microfibers with excellent mechanical properties in wearable devices are essential for practical application. **Figure S2b, c** shows Young's modulus and ultimate strength of the different mass ratios of GE/CNFs microfibers. As the increase CNFs mass ratios of GE/CNFs microfibers (from 1:0 to 1:0.75), tensile strength improves from 296 MPa to 423 MPa (an increase of 42.9%) and Young's modulus increased from 8.2 GPa to 14.34 GPa. These results are attributed to the uniform dispersion of the CNFs in the hybrid microfibers and the improved interfacial interaction (Hydrogen bonding) between CNFs and GE. However, when the CNFs ratios of GE increase to 1:1, the tensile strength and Young's modulus are significantly reduced. It may be due to a large number of CNFs increase the interspaces between the adjacent graphene layers, leading to a decrease in mechanical properties.[6]

Schematic diagram of the electrochemical test of the two-electrode aqueous microfiber supercapacitor (AQMFSC) system is shown in **Figure S1d**. For the Cyclic voltammetry (CV) test at the scan rate of 50 mV s^{-1} **(Figure S2d)**, the curve with the low area of the GE microfiber indicated an area capacitance of only 14 mF cm^{-2}. However, the area of the curve of GE/CNFs AQMFSC increased significantly, reached the highest area capacitance of 125 mF cm^{-2} for GE/CNFs 1:0.75 microfiber (capacitance performance increased by 9 times). **Figure S3 a-f** shows the CV curves of AQMFSCs with different CNFs content. According to compare the changes in area capacitance and capacitance retention of GE/CNFs microfiber electrodes at different scan rates **(Figure S1e and S3f)**, which is found that with the scan rate increase (from 5 mV s^{-1} -100 mV s^{-1}), GE and GE/CNFs microfiber electrodes all shows capacitance decrease. Notably, although GE/CNFs 1:0.75 microfiber electrode has the best capacitance retention rate of 42.92%, it has the most significant decrease in capacitance. Which may be caused by the limited conductivity of CNFs makes the electrochemical kinetics performance weak. When the scan rate is 10 mV s^{-1}, the

GE/CNFs 1:0.75 microfiber electrode has a maximum area-specific capacitance of 185 mF cm^{-2}. This is because the addition of the hydrophilic CNFs can effectively enhance the hydrophilicity of the GE/CNFs composite microfibers and promote the absorption and internal diffusion of electrolyte ions on the microfibers. Besides, the nano proppant CNFs effectively increases the layer spacing of the GE sheets. The internal surface area of the microfibers increases and more electrolyte ions can enter the microfibers and bind entirely to the exposed oxygen-containing groups inside the microfibers.[7] By comparing the sectional SEM image of GE microfiber and GE/CNFs 1:0.75 microfiber at the same high magnification **(Figure S4)**, it is finding that the interlayer spacing of the graphene sheets is significantly increased. We comprehensively compared the mechanical and electrochemical properties of the microfibers and found that GE/CNFs 1:0.75 microfiber has the highest mechanical strength (423 MPa) and capacitive properties (185 mF cm^{-2} at a scan rate of 10 mV s^{-1}). In summary, GE/CNFs 1:0.75 microfibers were selected as the core structure to prepare the GE/CNFs@PANI core-sheath microfibers.

Synthesis of Polyaniline Nanorods Arrays

According to controlling the reaction time, different morphologies of Polyaniline nanorod arrays were grown on the surface of GE/CNFs microfibers. **Figure S5a** illustrates the principle of in situ polymerization growth of polyaniline nanorod arrays. The detailed steps are as follows: first, 5-sulfosalicylic acid is ionized and releases H^+ in aqueous solution to protonated aniline **(compound a: $Ph\text{-}NH_2$)** to benzo ammonium cation **(compound b: $Ph\text{-}NH_3^+$)**; then **compound b** is oxidized to form an aniline nitrenium cation **(compound c: $Ph\text{-}NH^+$)** after the addition of persulfate and two protons are generated when **compound c** reacts with persulfate.[8] The p-position of the free aniline molecule in the solution would be attacked by aniline nitrenium cation and then forms a dimer of aniline **(compound d)** and releasing a proton.[9] Similarly, **compound d** forms its conjugated acid **(compound e)** by trapping protons in solution which is then oxidized to form a trimer **(compound f)**, generating protons. Through this acidification-oxidation-polymerization route, the monomeric aniline is polymerized into macromolecular polyaniline **(compound g)**. When each aniline molecule is polymerized, one proton is consumed but three protons are produced; the pH of the solution gradually becomes lower as the reaction progresses.[10] Concurrently, in the presence of oxidant persulfate, the fully reduced form of polyaniline **(compound g)** is effortless to convert into oxidized form **(compound h)**. As shown in **Figure S5b**, we control the chemical polymerizations of PANI in GE/CNFs microfiber with 4 h, 6 h, 8 h, 10 h, 12 h, and 24 h. After 4 h, PANI nanorods were grown on GE/CNFs microfibers successfully. However, the morphology of the polyaniline nanorods were not fully formed and the spacing among them were large. When chemically polymerized for 10 h, uniform arrays of vertical nanorods were formed on the GE/CNFs microfibers. Conversely, when the polymerization time over 12 h, the polyaniline exhibits an overgrowth state on the GE/CNFs microfibers.

Supplementary Figures

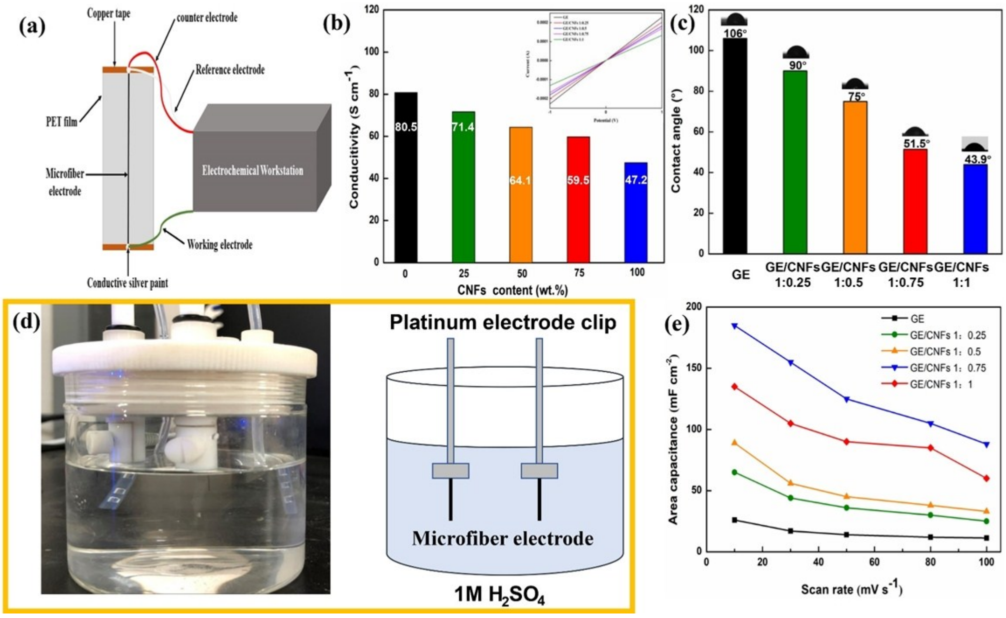

Figure S1. (a) Schematic diagram of conductivity test of GE/CNFs microfibers. (b) Conductivity change diagram of GE/CNFs microfibers. (c) Contact angle variation of GE/CNFs microfibers. (d) Schematic diagram of electrochemical test of two electrode aqueous microfiber supercapacitors. (e) Capacitance change based on the different scan rates of the GE and GE/CNFs microfibers.

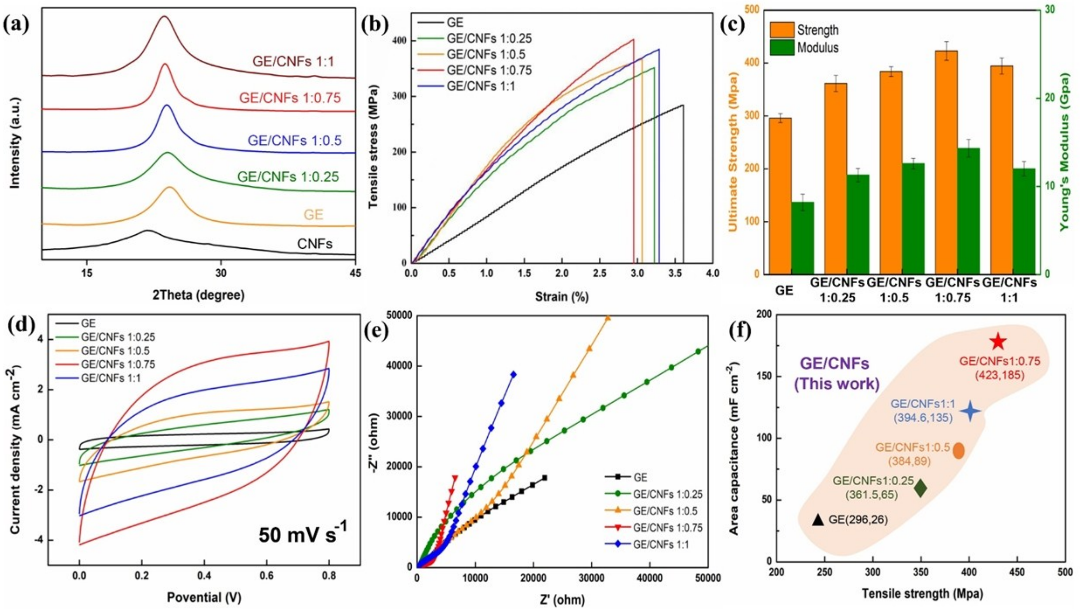

Figure S2. (a) XRD patterns of GE/CNFs microfiber with different CNFs contents. (b) Stress-strain curves of GE/CNFs microfibers. (c) Tensile strength and Young's modulus of GE/CNFs microfibers. (d) CV curves at 50 mV s^{-1} of the GE AQMFSC and GE/CNFs AQMFSCs. (e) Nyquist plots of GE and GE/CNFs AQMFSCs. (f) Comparison of the capacitance versus mechanical strength of GE/CNFs microfibers with different CNFs contents.

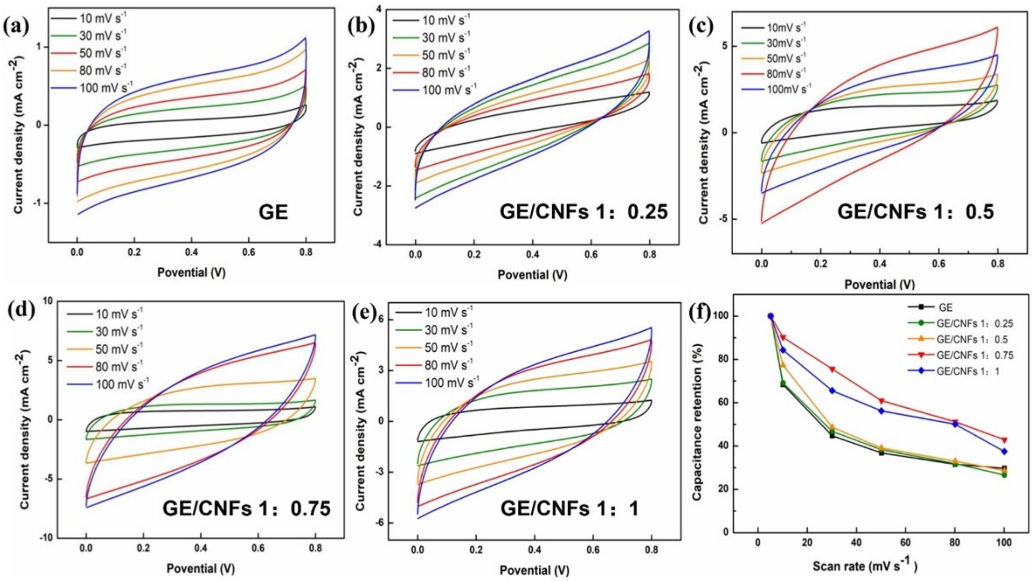

Figure S3. (a-e) CV curves of the GE AQMFSC and GE/CNFs AQMFSCs at different scan rates. (f) Capacitance retention ratio based on the scan rates of the GE AQMFSC and GE/CNFs AQMFSCs.

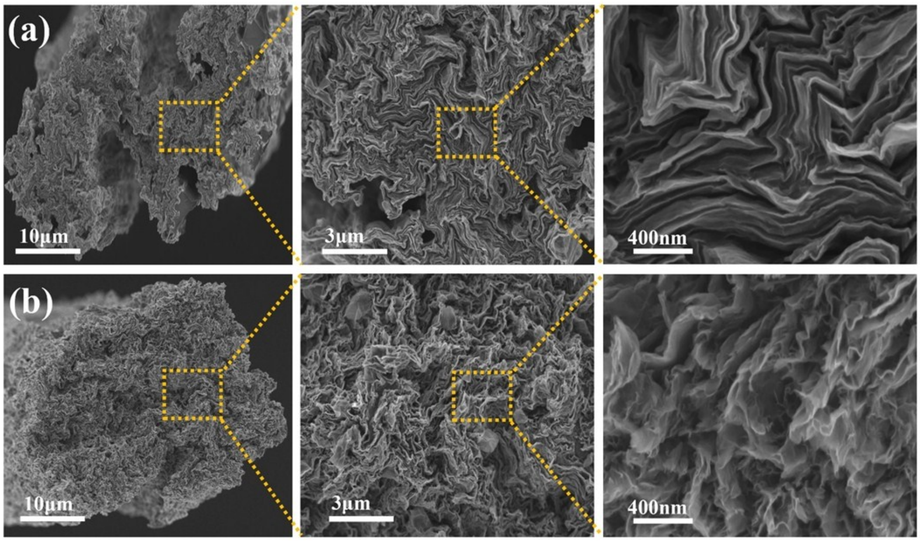

Figure S4. (a) Different magnifications cross-sectional SEM images of GE microfiber. (b) Different magnifications cross-sectional SEM images of GE/CNFs 1:0.75 composite microfibers.

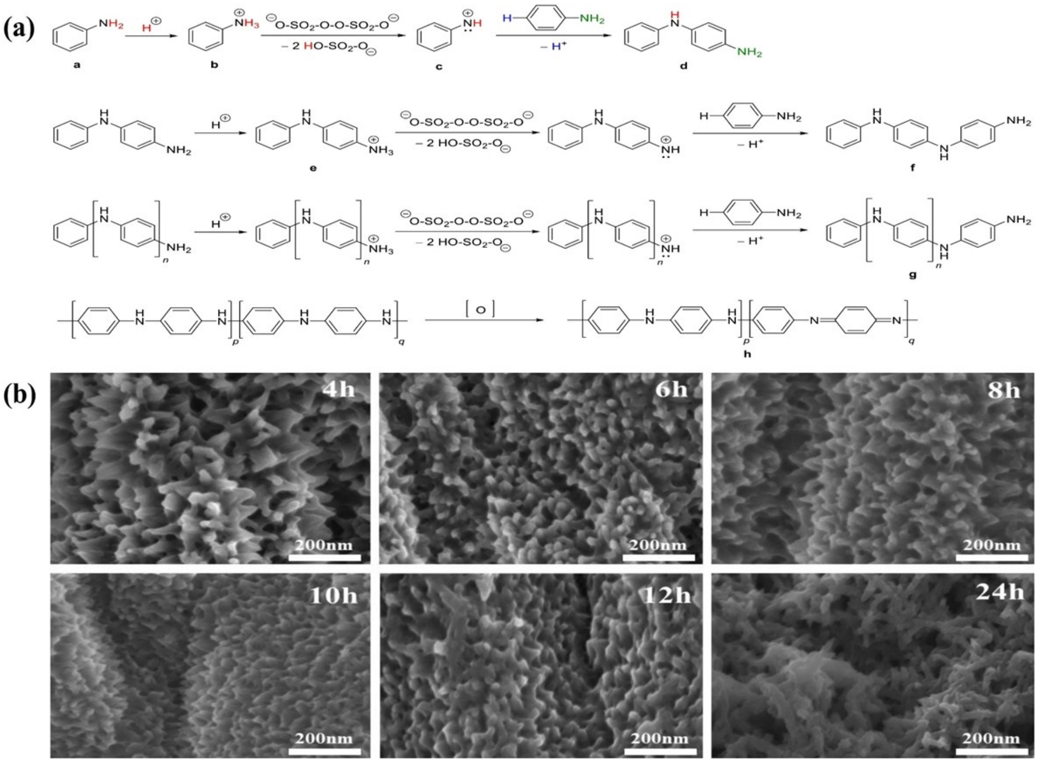

Figure S5. (a) Schematic illustration of in-situ polymerization growth of PANI nanorod arrays process. (b) PANI nanorod morphology on the surface of GE/CNFs@PANI microfibers at different polymerization times.

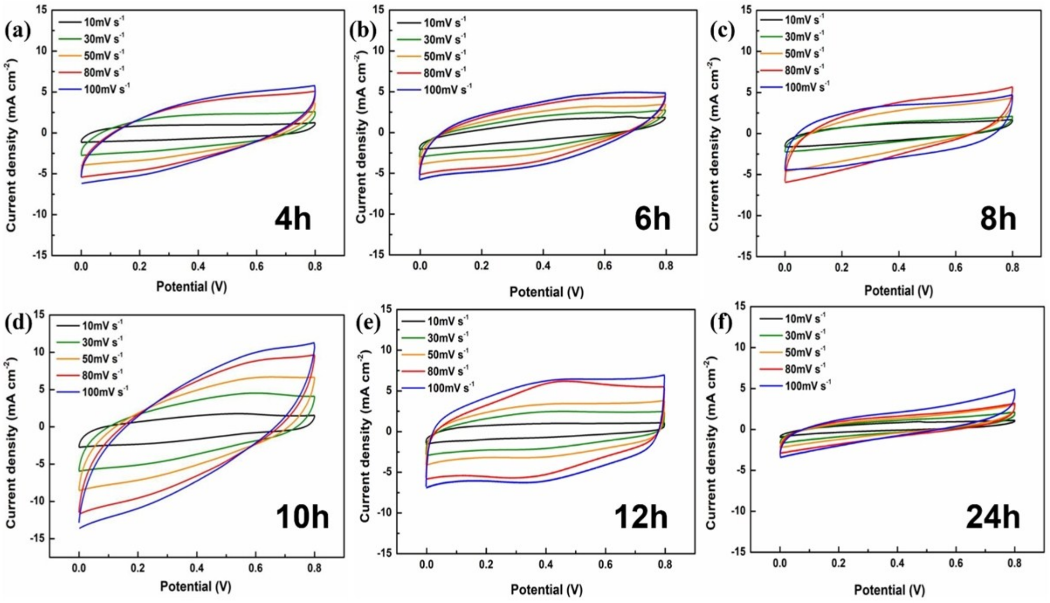

Figure S6. (a-f) CV curves of the GE@PANI AQMFSCs at different scan rates.

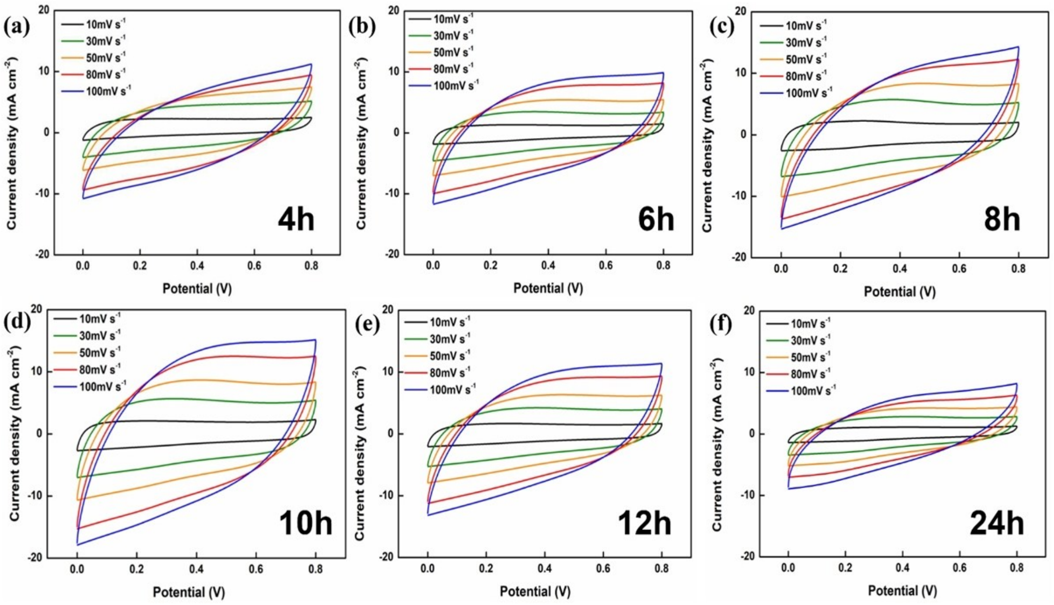

Figure S7. (a-f) CV curves of the GE/CNFs@PANI AQMFSCs at different scan rates.

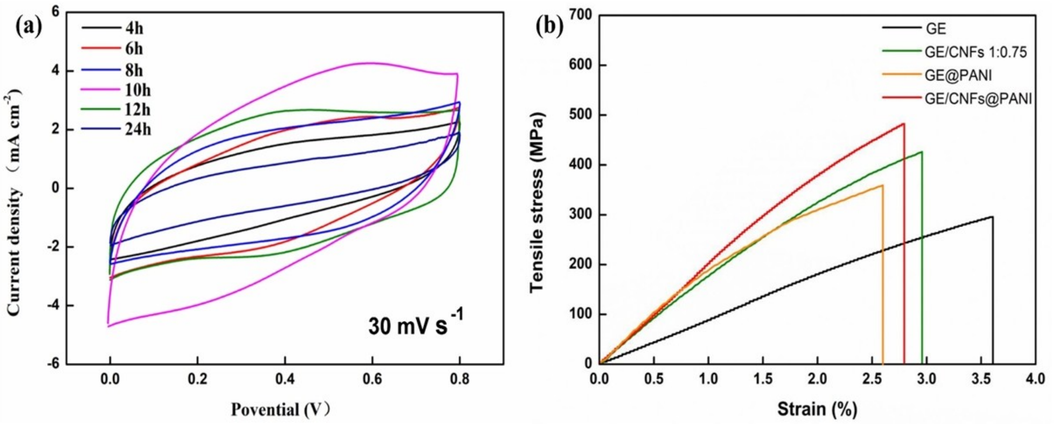

Figure S8: (a) Cyclic voltammetry curves of GE@PANI AQMFSCs at different polymerization times. (b) Strain–stress curves of GE, GE/CNFs 1:0.75, GE@PANI and GE/CNFs@PANI-10h microfibers.

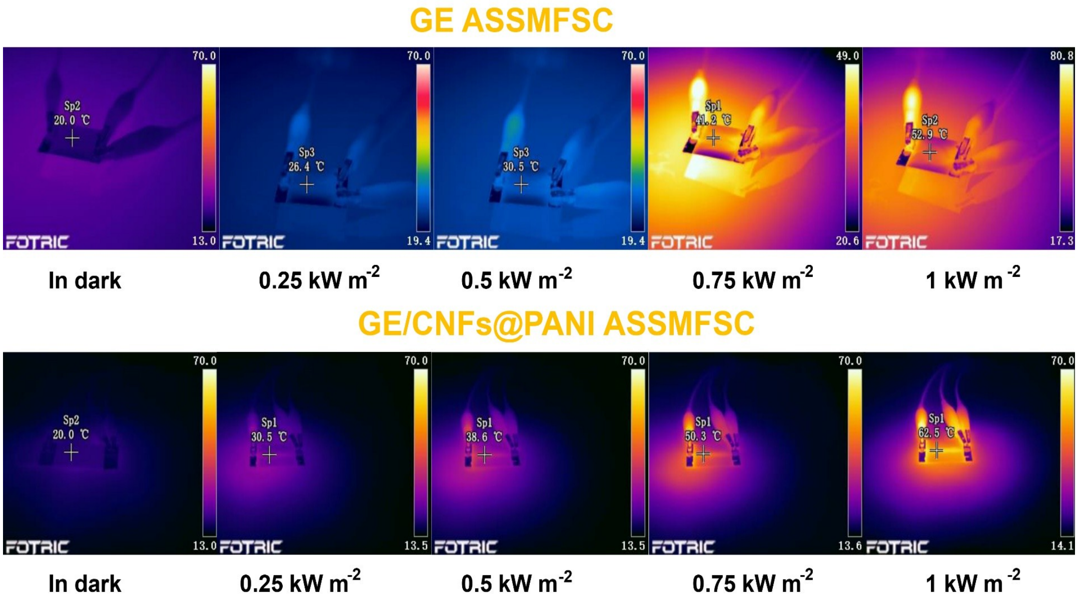

Figure S9. Infrared images of temperature changes of GE ASSMFSC and GE/CNFs@PANI ASSMFSC in the dark and different solar power densities.

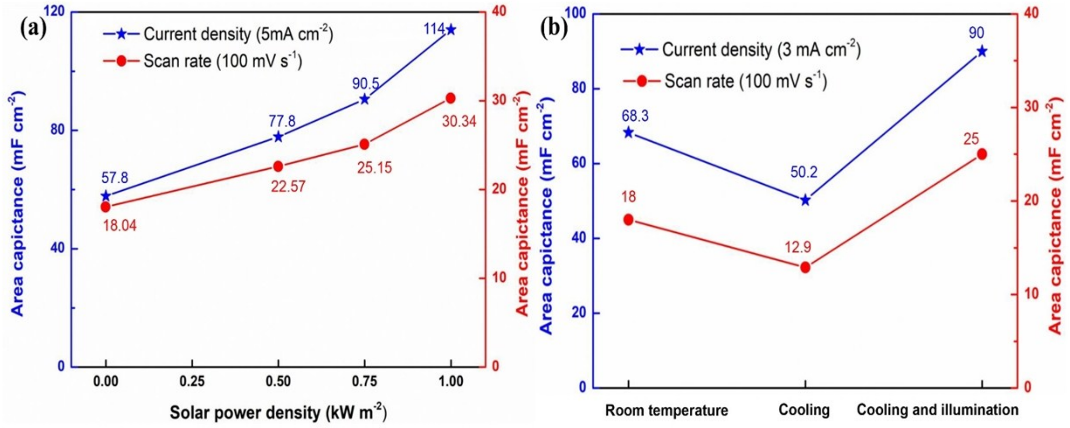

Figure S10. (a, b) Area capacitances of the whole GE/CNFs@PANI ASSMFSC calculated from the CV curves and GCD curves under different solar power densities and environmental temperatures.

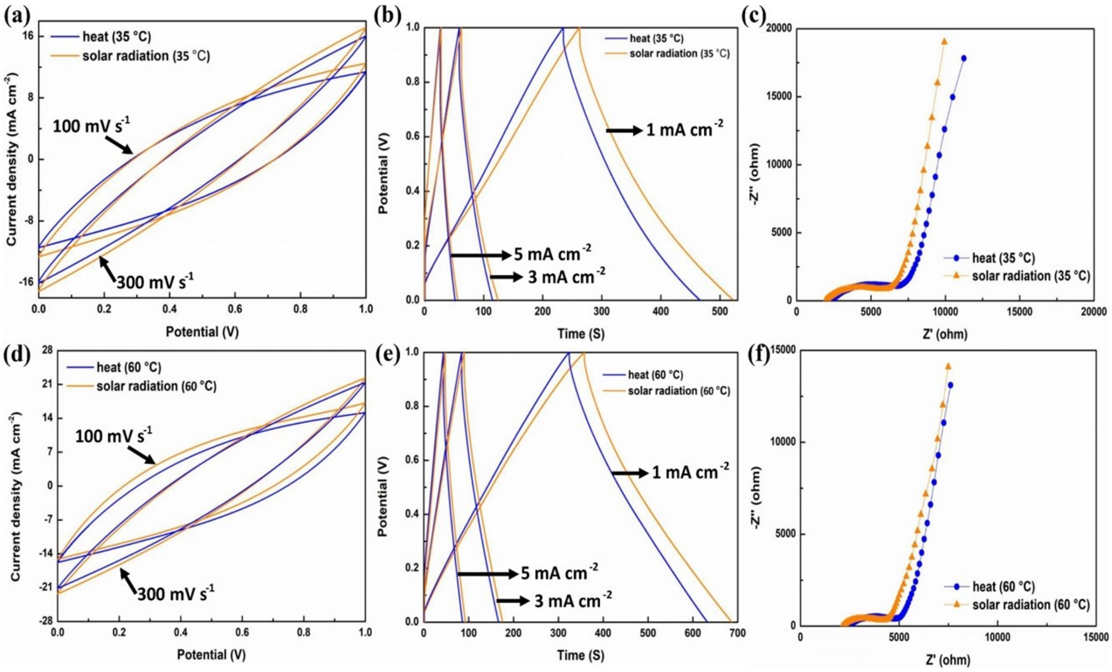

Figure S11. CV curves (a, d), GCD curves (b, e) and Nyquist plots (c, f) of the GE/CNFs@PANI ASSMFSC generated by heating and simulated sunlight.

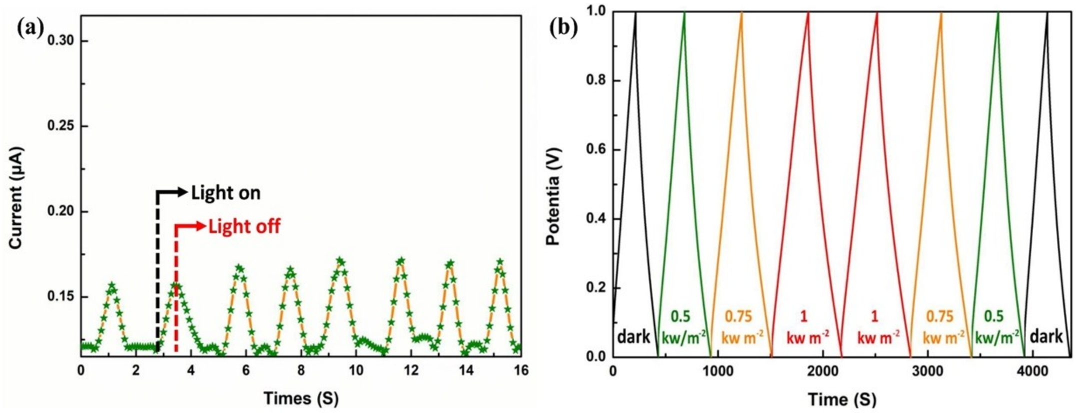

Figure S12. (a) Sunlight-responsive potentiostatic charge/discharge curves of GE/CNFs@PANI ASSMFSC in the dark and under sunlight (0.5 kW m^{-2}, 1 V). (b) Galvanostatic charge/discharge curves of GE/CNFs@PANI ASSMFSC at a current density of 1 mA cm^{-2} under different solar power density.

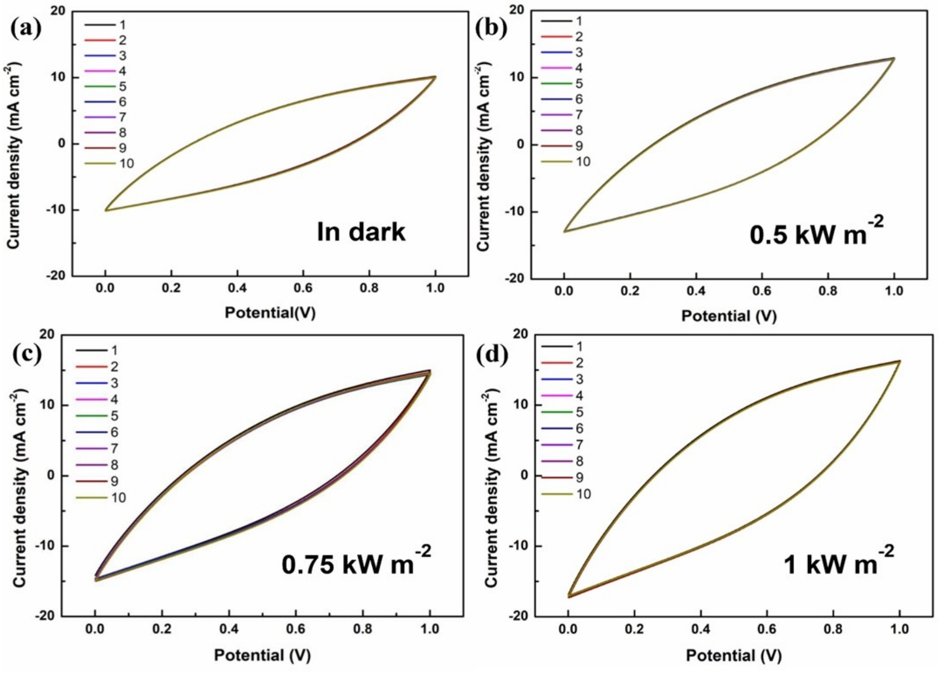

Figure S13. CV curves of GE/CNFs@PANI ASSMFSC at a scan rate of 100 mV s^{-1} under different solar power densities.

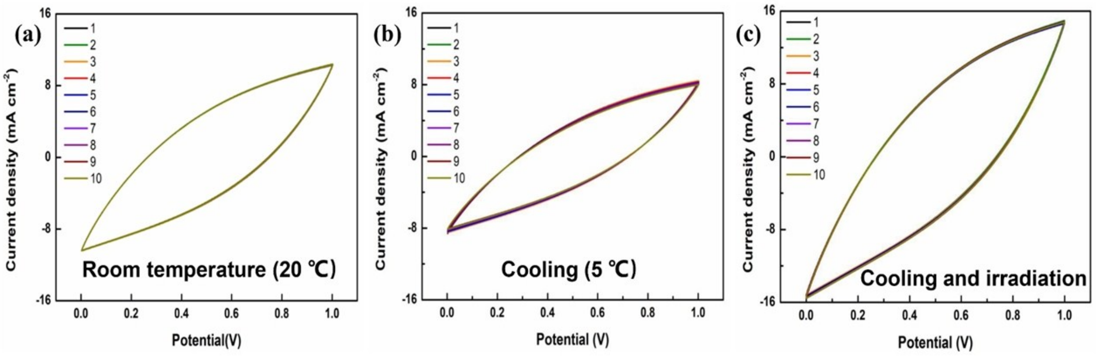

Figure S14. CV curves of GE/CNFs@PANI ASSMFSC at a scan rate of 100 mV s^{-1} under different environmental conditions.

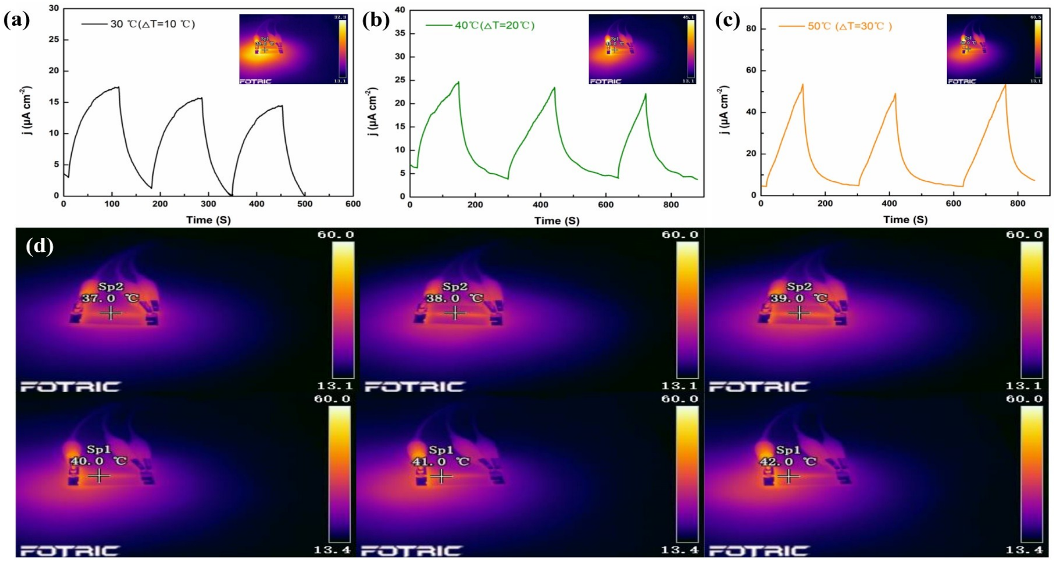

Figure S15. (a-c) Current change of ASSMFSC under different environment temperature at 1V constant voltage. Inset: Infrared images of ASSMFSC at different environment temperatures. (d) Infrared temperature of ASSMFSC during simulated human body temperature monitoring experiment.

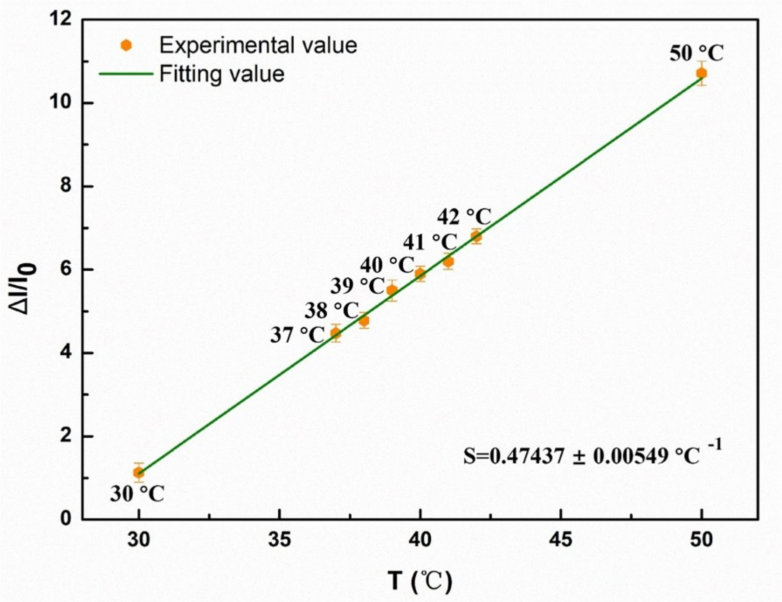

Figure S16. Normalized current change of the ASSMFSC at temperature ranging from 30 to 50 °C. Here, ΔI = I-I_0, where I_0 and I are the currents at 20 °C and at temperatures between 30 and 50 °C, respectively.

Table S1: Summary on the parameters of different microfibers.

Samples	Cross-sectional area (μm^2)	cross-sectional perimeter (μm)
GE microfiber	947.01 ± 18.3	176.47 ± 3.8
GE/CNFs 1:0.25 microfiber	1003.61 ± 8.5	156.96 ± 2.4
GE/CNFs 1:0.5 microfiber	1132.57 ± 12.2	168.39 ± 2.3
GE/CNFs 1:0.75 microfiber	1548.98 ± 13.2	151.92 ± 1.3
GE/CNFs 1:1 microfiber	1629.33 ± 12.6	187.22 ± 3.9
GE@PANI-4h microfiber	979.52 ± 16.1	182.08 ± 2.8
GE@PANI-6h microfiber	1189.99 ± 14.2	177.26 ± 4.2
GE@PANI-8h microfiber	1228.69 ± 18.4	183.17 ± 5.2
GE@PANI-10h microfiber	1304.59 ± 8.9	185.25 ± 2.6
GE@PANI-12h microfiber	1263.14 ± 12.3	192.52 ± 3.1
GE@PANI-24h microfiber	1302.32 ± 16.9	176.01 ± 4.7
GE/CNFs@PANI-4h microfiber	1436.69 ± 18.1	160.34 ± 1.9
GE/CNFs@PANI-6h microfiber	1695.42 ± 13.3	154.44 ± 2.5
GE/CNFs@PANI-8h microfiber	1979.52 ± 9.5	169.33 ± 1.5
GE/CNFs@PANI-10h microfiber	1789.63 ± 18.7	145.59 ± 2.9
GE/CNFs@PANI-12h microfiber	2006.28 ± 14.6	166.78 ± 6.4
GE/CNFs@PANI-24h microfiber	2200.97 ± 9.6	161.85 ± 2.2

Table S2: Mechanical properties of the GE/CNFs@PANI microfiber compared with some previously reported MFSCs electrodes.

Microfiber materials	Strength (MPa)	Strain (%)	Reference
Polypyrrole@ CNFs	60	1.2	[11]
SWNT/active carbon	76	0.7	[12]
N-doped RGO/SWNT	84-165	3.3-3.9	[13]
GF@3D-G	155	2.1	[14]
VN/CNT	370	2.0	[15]
RGO/PANI	183.7	2.5	[16]
CNFs-RGO/PPY	364.3	2.9	[17]
Plasma Treatment RGO	280	2.0	[18]
RGO/Mn_3O_4	60-95	3.1-6	[19]
RGO/CNC	230	4.1	[20]
RGO/MXene	140	3.8	[21]
MnO_2/Ti_3C_2Tx/RGO	20	9	[22]
RGO/ MnO_2	160	7	[23]
GE/CNFs@PANI	**476.25**	**3.65**	**This work**

Table S3: Electrochemical parameters of the GE/CNFs@PANI ASSMFSC compared with some reported fiber-shaped energy storage devices.

electrode materials	device setting	electrolyte	energy density (mWh cm^{-3})	power density (W cm^{-3})	reference
PEDOT-S: PSS	parallel	PVA/H_2SO_4	8.3	0.002	[24]
Graphene fibers	parallel	PVA/H_3PO_4	6.30	0.013	[13]
RGO/CNFs/PPY	twisted	PVA/H_3PO_4	4.80	0.0158	[17]
Ti/TiO_2/MoS_2	twisted	PVA/H_3PO_4	4.98	0.05	[25]
CuO@CoFe-LDH	twisted	PVA/KOH	1.86	0.17	[26]
RGO/Ni cotton	parallel	PVA/LiCl	6.10	0.35	[27]
RGO/CNC	parallel	PVA/H_2SO_4	5.10	0.4964	[20]
Polymer fibers	parallel	PVA/H_3PO_4	3.20	0.03	[28]
Ni_3S_2 nanowire	coaxial	PVA/KOH	0.81	0.02	[29]
CNT/MnO_2 yarn	twisted	PVA/KOH	3.52	0.13	[30]
MnO_2/carbon	parallel	PVA/H_3PO_4	0.22	0.40	[31]
Au/RuO_2	parallel	PVA/H_3PO_4	10.1	0.0012	[32]
PANI/RGO fiber	parallel	PVA/H_2SO_4	8.80	0.031	[33]
PPY/RGO/CNT	parallel	PVA/H_3PO_4	0.94	0.1171	[34]
GE/CNT@CMC	twisted	PVA/H_3PO_4	3.5	0.0018	[35]
PPY/MnO_2/RGO	parallel	PVA/H_3PO_4	1.1	0.110	[36]
MnO_2/CNT fiber	parallel	PVA/KOH	0.69	0.260	[37]
RGO/AC fiber	parallel	PVA/H_3PO_4	2.5	0.10	[38]
GE/CNFs@PANI	**twisted**	**PVA/H_2SO_4**	**11.9**	**0.022**	**This work**

Table S4: Normalized current obtained from the GE/CNFs@PANI ASSMFSC at different temperatures from 30 to 50 °C.

Temperature (K)	**Temperature (°C)**	**normalized current ($\Delta I/I_0$)**
315.15	30	1.128±0.23
310.15	37	4.474±0.21
311.15	38	4.78±0.19
312.15	39	5.5±0.25
313.15	40	5.9±0.18
314.15	41	6.2±0.19
315.15	42	6.8±0.22
323.15	50	10.714±0.31

Reference

1. W. S. H. Jr and R. E. Offeman, *J.am.chem.soc*, 1958, **80**, 1339.
2. Y. Xu, K. Sheng, C. Li and G. Shi, *Acs Nano*, 2010, **4**, 4324-4330.
3. K. Abe and H. Yano, *Carbohydrate Polymers*, 2011, **85**, 733-737.
4. K. Abe, S. Iwamoto and H. Yano, *Biomacromolecules*, 2007, **8**, 3276-3278.
5. G. Wang, B. Wang, J. Park, J. Yang, X. Shen and J. Yao, *Carbon*, 2009, **47**, 68-72.
6. C. Choi, J. H. Kim, H. J. Sim, J. Di, R. H. Baughman and S. J. Kim, *Advanced Energy Materials*, 2017, **7**, 388-412.
7. L. Yun, Z. Jie, T. Jian and W. Tang, *Chemistry of Materials*, 2015, **27**, 150930173019006.
8. Z. Tai, X. Yan and Q. Xue, *Journal of The Electrochemical Society*, 2012, **159 (10)**, A1702-A1709.
9. Z. Kai, L. Zhang, S. Zhao and J. Wu, Chemistry of Materials, 2010, **22**, 1392-1401.
10. G. Ćirić-Marjanović, E. N. Konyushenko, M. Trchová and J. Stejskal, *Synthetic Metals*, 2008, **158**, 200-211.
11. N. Sheng, S. Chen, J. Yao, F. Guan, M. Zhang, B. Wang, Z. Wu, P. Ji and H. Wang, Chemical Engineering Journal, 2019, **368**, 1022-1032.
12. Q. Meng, H. Wu, Y. Meng, K. Xie, Z. Wei and Z. Guo, Advanced Materials, 2014, **26**, 4100-4106.
13. D. Yu, K. Goh, H. Wang, L. Wei, W. Jiang, Q. Zhang, L. Dai and Y. Chen, Nature Nanotechnology, 2014, **9**, 555.
14. Y. N. Meng, Y. Zhao, C. G. Hu, H. H. Cheng, Y. Hu, Z. P. Zhang, G. Q. Shi and L. T. Qu, Advanced Materials, 2013, **25**, 2326-2331.
15. Q. Zhang, X. Wang, Z. Pan, J. Sun, J. Zhao, J. Zhang, C. Zhang, L. Tang, J. Luo and B. Song, Nano Letters, 2017, **17**, 2719.
16. D. Liu, J. Liu, Q. Wang, P. Du, W. Wei and P. Liu, Carbon, 2019, **143**, 147-153.
17. M. Mo, C. Chen, G. Han, M. Chen and D. Li, Electrochimica Acta, 2018, **269**, 11-20.
18. J. Meng, W. Nie, K. Zhang, F. Xu, X. Ding, S. Wang and Y. Qiu, Acs Applied Materials & Interfaces, 2018, **10**, 13652.
19. S. Chen, L. Wang, M. Huang, L. Kang, Z. Lei, H. Xu, F. Shi and Z. H. Liu, Electrochimica Acta, 2017, **242**, 10-18.

20. G. Chen, C. Tao, H. Kai, W. Ma, M. Tebyetekerwa, Y. Cheng, W. Wei and M. Zhu, Carbon, 2018, **127**, 218-227.

21. Q. Yang, X. Zhen, F. Bo, T. Huang and G. Chao, Journal of Materials Chemistry A, 2017, **5**, 10.1039.C1037TA07999K.

22. M. Lu, Z. Zhang, L. Kang, X. He, Q. Li, J. Sun, R. Jiang, H. Xu, F. Shi, Z. Lei and Z.-H. Liu, Journal of Materials Chemistry A, 2019, **7**, 12582-12592.

23. B. Zheng, T. Huang, L. Kou, X. Zhao, K. Gopalsamy and C. Gao, J. Mater. Chem. A, 2014, **2**, 9736-9743.

24. Z. Wang, J. Cheng, Q. Guan, H. Huang, Y. Li, J. Zhou, W. Ni, B. Wang, S. He and H. Peng, Nano Energy, 2018, **45**, 210-219.

25. L. Huang, J. Cheng, X. Li, D. Yuan, W. Ni, G. Qu, Q. Guan, Y. Zhang and B. Wang, Journal of Materials Chemistry A, 2015, **3**, 4049-4057.

26. Z. Li, M. Shao, Z. Lei, R. Zhang, Z. Cong, J. Han, W. Min, D. G. Evans and D. Xue, *Nano Energy*, 2016, **20**, S2211285516000021.

27. L. Liu, Y. Yu, C. Yan, K. Li and Z. Zheng, Nature Communications, 2015, **6**, 7260.

28. G. Qu, J. Cheng, X. Li, D. Yuan, P. Chen, X. Chen, B. Wang and H. Peng, Advanced Materials, 2016, **28**, 3646-3652.

29. W. Jian, S. Li, Z. Kai, Z. Song, B. Li, C. Zhao, C. Tian, Y. Guo and G. Fang, Journal of Power Sources, 2016, **324**, 325-333.

30. C. Changsoon, L. Jae Ah, C. A Young, K. Youn Tae, L. Xavier, M. D. Lima, R. H. Baughman and K. Seon Jeong, Advanced Materials, 2014, **26**, 2059-2065.

31. X. Xiao, T. Li, P. Yang, Y. Gao, H. Jin, W. Ni, W. Zhan, X. Zhang, Y. Cao and J. Zhong, Acs Nano, 2012, **6**, 9200-9206.

32. K. Brousse, S. Pinaud, S. Nguyen, P. F. Fazzini, R. Makarem, C. Josse, Y. Thimont, B. Chaudret P. L. Taberna, M. Respaud, P. Simon, Advanced Materials, 2020, **11**, 1903136.

33. P. Li, Z. Jin, L. Peng, F. Zhao, D. Xiao, Y. Jin and G. Yu, Advanced Materials, 2018, **30**, e1800124.

34. S. Wang, N. Liu, J. Su, L. Li, F. Long, Z. Zou, X. Jiang and Y. Gao, Acs Nano, 2017, **11**, 2066.

35. L. Kou, T. Huang, B. Zheng, Y. Han, X. Zhao, K. Gopalsamy, H. Sun and C. Gao, Nature Communications, 2014, **5**, 3754.

36. Y. Huang, H. Hu, Y. Huang, M. Zhu, W. Meng, Z. Pei, C. Liu and C. Zhi, Acs Nano, 2015, **9**, 4766.

37. P. Xu, B. Wei, Z. Cao, J. Zheng, K. Gong, F. Li, J. Yu, Q. Li, W. Lu and J. H. Byun, Acs Nano, 2015, **9**, 6088-6096.

38. W. Ma, S. Chen, S. Yang, W. Chen, W. Weng and M. Zhu, Acs Appl Mater Interfaces, 2016, **8**, 14622-14627.